Rensselaer Polytechnic Institute

Troy, New York 12181

DISCLAIMER

DISCLAIMER

Portions of this document may be illegible in electronic image products. Images are produced from the best available original document.

21,611

LINEAR ACCELERATOR PROJECT

AEC Contract No. AT(11-1)-3058

PROGRESS REPORT

for

January 1, 1973 - March 31, 1973

Rensselaer Polytechnic Institute
Troy, New York 12181

Erwin R. Gaerttner
Project Director

MASTER

TABLE OF CONTENTS

Page

NEUTRON CROSS SECTIONS

RESONANCE AND THERMAL $\bar{\nu}$ MEASUREMENTS ON ^{239}PU

R. W. Hockenbury, R. L. Reed and R. C. Block

The following abstract was submitted to the Third Symposium on the Physics and Chemistry of Fission, to be held in Rochester, New York, August 13-17, 1973.

ABSTRACT

The prompt fission neutron average multiplicity $\bar{\nu}$ of ^{239}Pu has been measured at the RPI LINAC from 0.01 to 100 eV, using a fission chamber and a 0.75 meter diameter Gd-loaded liquid scintillator. Values of $\bar{\nu}$ have been determined for 22 resonances with standard deviations ranging from 0.2 to 0.5%. The $\bar{\nu}$ values fluctuate significantly from resonance to resonance, and statistical tests of the values indicate that their distribution is consistent with two or more populations. There is a tendency for higher $\bar{\nu}$ values to be associated with resonances with spin $J = 0^+$, while almost all the lower values correspond to resonances of spin $J = 1^+$. In the 0.3 to 0.01 eV range, $\bar{\nu}$ increases with decreasing energy, with $\bar{\nu}$ for the 0.3 eV resonance significantly lower than the value at 0.0253 eV. From 0.10 to 0.011 eV, $\bar{\nu}$ increases with a slope of approximately 0.6%. These new data follow the same trend with resonance energy as the earlier results of Weinstein et al. if their data in the 40 to 100 eV region are renormalized downward slightly. Comparisons have also been made to recent measurements at Oak Ridge and Saclay. In the resonance region, our results also show the same trend with resonance energy as the results reported by Oak Ridge, but the Oak Ridge $\bar{\nu}$ values do not show the tendency to divide into groupings as do the RPI and Saclay data. On the other hand, our results do not show the same trend with energy as the Saclay results, and in particular, there is a strong reversal in the two sets of data for the $\bar{\nu}$ values of the 41.4 and 44.6 eV resonances.

HIGH RESOLUTION CAPTURE AND TOTAL CROSS SECTIONS OF ^{54}FE AND ^{61}NI

H. D. Knox, M. Costello, R. W. Hockenbury and R. C. Block

With the large neutron flux available after the installation of the Model 12 electron gun, high resolution capture and total cross section measurements of ^{54}Fe and ^{61}Ni have been undertaken. The neutron energy range of interest in these experiments is between approximately 10 and 200 keV.

The 1.25-meter diameter capture tank at a 25-meter flight path and the ^{10}B NaI detector at a 28-meter flight path are being used in these measurements. Using an 11 nsec electron pulse, a 7.7 nsec channel width and including the effects of the moderator and sample thickness, the overall timing resolution of the system is approximately 19 nsec. The capture and transmission samples are cycled throughout the data taking so as to average the effects of variations in neutron intensity.

The capture measurements have been completed and the transmission measurements are under way. Preliminary analysis of the capture data shows that the resonance at 17.7 and 21.3 keV in ^{61}Ni reported in earlier lower resolution capture measurements[1] are doublets.

REFERENCE:

1. Linear Accelerator Project Annual Technical Report, October 1, 1971 - September 30, 1972, COO-3058-27.

^{60}NI (n,E$_\gamma$) DATA ANALYSIS (PRELIMINARY)

P. Brown,[*] J. R. Tatarczuk and R. C. Block

An experiment was performed using the RPI LINAC to determine
the spectrum of gamma rays emitted following neutron capture in a
separated ^{60}Ni isotope ($\approx$50 gm). The gamma ray spectrum was in-
vestigated as a function of neutron energy. A Ge(Li) detector
(55 cm^3 nominal active volume) was used to detect the capture
events at a flight path of 12.65 m. The data (25 time-of-flight
regions, each containing 2048 channels of pulse-height data) were
analyzed by an 8192 channel ADC and a 62.5 nsec time-of-flight
clock. The data were stored on-line on a PDP-9 computer disk in
a two-parameter array specifying the gamma ray energy and the
corresponding neutron time-of-flight region.

The data accumulation required approximately 100 hours of
linac time. The linac beam parameters were as follows: width
50 nsec, rep. rate 500 Hz, average current 26 μA, energy 70 MeV.
The low average current (because of the Model 10 electron gun)
yielded a very low stored count rate of $\approx$18/sec.

Useful data were obtained for the transitions to the ground
state (GS, E$_\gamma$ = 7.817 MeV) and second excited state (E$_\gamma$ = 7.534
MeV) in 11 time-of-flight regions. These transitions are believed
to be E1 transitions, ($\frac{1}{2}$+ $\to$ (3/2-) and ($\frac{1}{2}$+) $\to$ ($\frac{1}{2}$-), respectively.
The neutron energy of these regions extends from the large s-wave
resonance at 12 keV down to 13 eV. The boundaries of these neu-
tron energy regions are shown in Table 1. In addition a previous
Cd difference experiment provided data on the GS and second ex-
cited state transition for thermal neutrons. The ratio of the GS
to the second excited state transitions is shown in Table 1 for
the neutron energy regions mentioned above. The large errors in
the ratios, typically 15% or greater, reflect the background un-
certainties as well as the counting statistics of the small num-
ber of counts observed under the γ-ray peaks. The low count rate
of the experiment yielded GS areas (above background) of typically
250 counts and second excited areas of typically 150 counts. The

---

[*]Based in part on the Ph.D. Thesis of P. Brown.

ratios in Table 1 show a disturbingly small X^2 when a weighted least squares analysis performed. The data are best fit by either a horizontal (weighted average) or a slightly sloped straight line. The horizontal line fit yields a ratio = 1.65 ± 0.03.

The p-wave resonance at 2.2 keV produces a strong transition to the first excited state (E_γ = 7.750 MeV). This is believed due to the gamma ray transition selection rules allowing an M1 or E2 transition from a p-wave capture state of ½- or 3/2- to the 5/2- first excited state. This first excited state transition is much stronger than either the GS or the second excited state transition in this neutron energy range (E_n = 2.18 - 2.34 keV). Also, the GS transition is smaller than the second excited state in this region. It has not been determined yet what percentage of the GS and second excited state transitions in this region result from p-wave capture (M1 or E2 transitions), and what percentage is due to the tail of the s-wave capture (E1 transitions) background which underlies the p-wave resonance. The analysis is continuing.

Data on natural iron have also been accumulated with better counting statistics than the ^{60}Ni data due to the installation of a new Model 12 electron gun. These data have not been analyzed as yet.

Table 1. Ratio GS/2nd Excited ^{60}Ni

Time-of-Flight Region (run 85)	Neutron Energy (eV)		Ratio		
7	17370	- 8242	1.52	±	.11
13	4574	- 2701	1.43	±	.60
17	1911	- 985.4	1.35	±	.40
18	981.2	- 545.3	1.48	±	.41
19	543.5	- 164.7	1.55	±	.21
20	164.4	- 92.01	1.56	±	.23
21	91.89	- 54.90	1.63	±	.24
22	54.84	- 34.58	1.60	±	.18
23	34.55	- 23.76	1.56	±	.19
24	23.74	- 17.32	1.38	±	.18
25	17.31	- 13.24	1.82	±	.25

Cd difference

Neutron energy: ≈0.03 eV - 0.01 eV
1.70 ± 0.04

Decay Scheme

^{60}Ni + n   7.817 MeV

½-   0.283 2nd excited

5/2-   0.067 1st excited
3/2-   0.000 GS
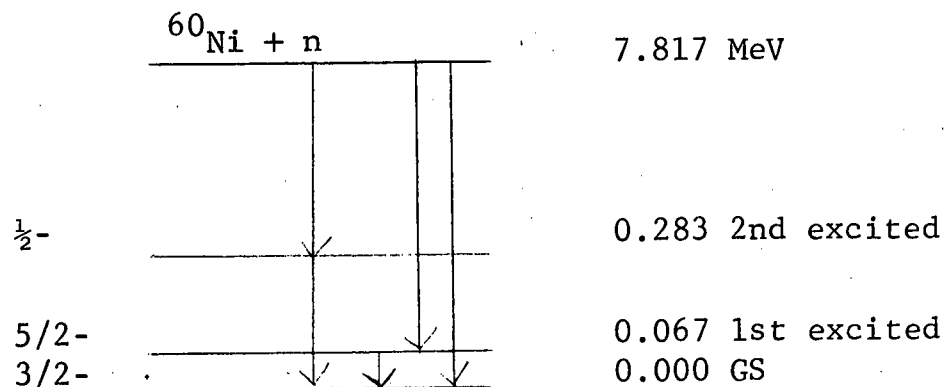
AVERAGE RESONANCE PARAMETERS OF DEPLETED URANIUM
AND TANTALUM IN THE ENERGY RANGE 10 TO 100 KEV[‡]

T. Y. Byoun,[*] R. C. Block and T. Semler[+]

The average resonance parameters of depleted uranium (99.8% ^{238}U and 0.2% ^{235}U) and tantalum have been obtained in the energy range from 10 to 100 keV. This is a part of the results completing the temperature dependent measurements of the average transmission, <TR>, and of the average self-indication ratio, <SIR>, upon depleted uranium and tantalum. The details of the measurements and of the calculational methods as well as the partial results have been presented in previous reports.[1,2,3]

The results are plotted in Figs. 1 and 2 in terms of <TR> and <SIR> for both depleted uranium and tantalum. The average resonance parameters which best fit the experimental results (<TR> and <SIR>) are listed in Table 1 (for uranium) and Table 2 (for tantalum).

Depleted Uranium

For the uranium analysis, the p-wave resonance parameters have been extensively studied by taking the experimental s-wave parameters available, which are listed in Table 1. As can be seen in Figs. 1a and 1b, and Table 1, the p-wave strength function, S_1, which best fits experimental results ranges from 1.27×10^{-4} to 2.4×10^{-4} for the corresponding variations of the scattering length, R', from 9.6 to 9.0 fermis. This suggests that the strength function is strongly dependent on R'. Since R' is directly related to the potential cross section, σ_p, accurate measurements of σ_p are necessary for a unique determination of the strength function.

Figures 3 and 4 show the sensitivity of <TR> and <SIR> to the scattering length and to the strength function respectively in the energy range from 37.3 to 33.8 keV.

According to Figs. 1a and 1b, the fits obtained using the three sets of parameters labeled A, B and C in Table 1 are almost identical and the choice of one of these three sets of parameters over another can be made only if very accurate potential cross sections are known.

It should be noted that the average self-indication ratios cannot be fit well using the conventional J-dependence formula for the level spacing which assumes parity independence:[4]

$$\langle D_{\ell J} \rangle = C(2J + 1)^{-1} \qquad (1)$$

$$= \langle D_{\ell' J} \rangle \text{ for } \ell \neq \ell' , \qquad (1')$$

and

$$\langle D_\ell \rangle = g_J \langle D_{\ell J} \rangle / \Sigma_{J'} g_{J'} , \qquad (2)$$

where C is assumed to be parity independent and the other notations are standard.

As can be seen in Table 1, the best fit p-wave level spacing, $\langle D_1 \rangle$, is 11.3 $\pm$ 3.0 eV, which is approximately 60% larger than $\langle D_1 \rangle$ from Eqs. (1) and (2). This difference could indicate a parity dependence of the level spacing. The fit obtained using the ENDF/B-III parameters ($\langle D_1 \rangle$ = 6.67 eV) predicts consistently higher (1.0 - 7.0%) values of <SIR> than experimental results as shown in Fig. 1a, while the prediction of <TR> by the ENDF/B parameters is in excellent agreement with experimental <TR> as shown in Fig. 1b.

If the level spacing and radiation width are increased while the capture strength function, $\overline{\Gamma}_{\nu \ell} / \langle D_{\ell J} \rangle$, is held constant, then the <SIR> decreases due to the increase of the cross section fluctuation even though the average capture cross section still remains the same. However, it is still difficult to conjecture that there is a definite parity dependence of the level spacing because:

1) The d-wave contribution to the capture cross section of ^{238}U is not negligible in the energy range from 30 to 100 keV.

2) The assumption of the spin independence of
   S_1 which is used in this analysis has yet
   to be considered.

3) The change in the predictions of <SIR> by
   applying the parity independence of level
   spacing is not greatly different from that
   obtained with the best fit parameters, con-
   sidering the experimental errors in <SIR>
   ($\pm 2.0\%$ of counting statistics plus $+2.0\%$
   of estimated systematic errors).

Tantalum

The average resonance parameters which best fit <TR> and <SIR>
of tantalum in the energy range from 10 keV to 100 keV are listed
in Table 2. The potential cross sections obtained using the scat-
tering length, $R' = 8.19$ fermi, range from 8.42 barns at 1.0 keV
to 7.80 barns at 100 keV, which is a little higher than the
measured value, $\sigma_p = 7.0 \pm 1.0$ barns.[5]

The average transmission and the average self-indication ratio in
the energy range from 1.0 keV to 100 keV are shown and compared
with the results of the analytical calculations[2] in Figs. 2a and
2b. According to these figures, the best fit s-wave strength
function, $S_o = 1.6 \times 10^{-4}$, is slightly lower than the previously
measured values, which range from $S_o = 1.8 \times 10^{-4}$ (with
$\overline{\Gamma}_{\gamma o} = 0.055$ eV and $<D_o> = 4.3$ eV)[6] to $S_o = 2.0 \times 10^{-4}$ (with
$S_1 = 0.2 \times 10^{-4}$, $<D_o> = 4.3$ eV and $\overline{\Gamma}_{\gamma o} = 0.065$ eV).[7] However, it
appears that in the energy range from 1 keV to 10 keV, a slightly
higher s-wave strength function ($S_o = 2.0 \times 10^{-4}$) fits better
both <TR> and <SIR> of the thinnest sample (0.00563 atom/barn) as
can be seen in Figs. 1a and 1b.

REFERENCES:

1. T. Y. Byoun, R. C. Block and T. Semler, Proc. Third Conf. on Neutron Cross Sections and Technology, CONF-710301, Vol. 2, March 1971.

2. T. Y. Byoun, R. C. Block and T. Semler, Proc. ANS Topical Meeting on New Development in Reactor Physics and Shielding, CONF-720901 (Book 2), September 1972.

3. Linear Accelerator Project Annual Technical Report, October 1, 1971 - September 30, 1972, COO-3058-27.

4. A. Gilbert and A. G. W. Cameron, Can. J. Phys. 43, 1965.

5. R. E. Wood, Phys. Rev. 104, No. 5, 1956.

6. J. S. Desjardins, et al, Phys. Rev. 120, 2214 (1960).

7. J. M. Gibbons, EANDC 1961 (Neutron TOF Method).

FIGURE CAPTIONS

Fig. 1a, 1b   The Average Transmission (1a) and the Average Self-indication Ratio (1b) of Depleted Uranium for Different Sample Thicknesses.

Fig. 2a, 2b   The Average Transmission (2a) and the Average Self-indication Ratio (2b) of Tantalum for Different Sample Thicknesses.

Fig. 3   The Sensitivity of <TR> and <SIR> of Depleted Uranium to the Strength Function.

Fig. 4   The Sensitivity of <TR> and <SIR> of Depleted Uranium to the Scattering Length.
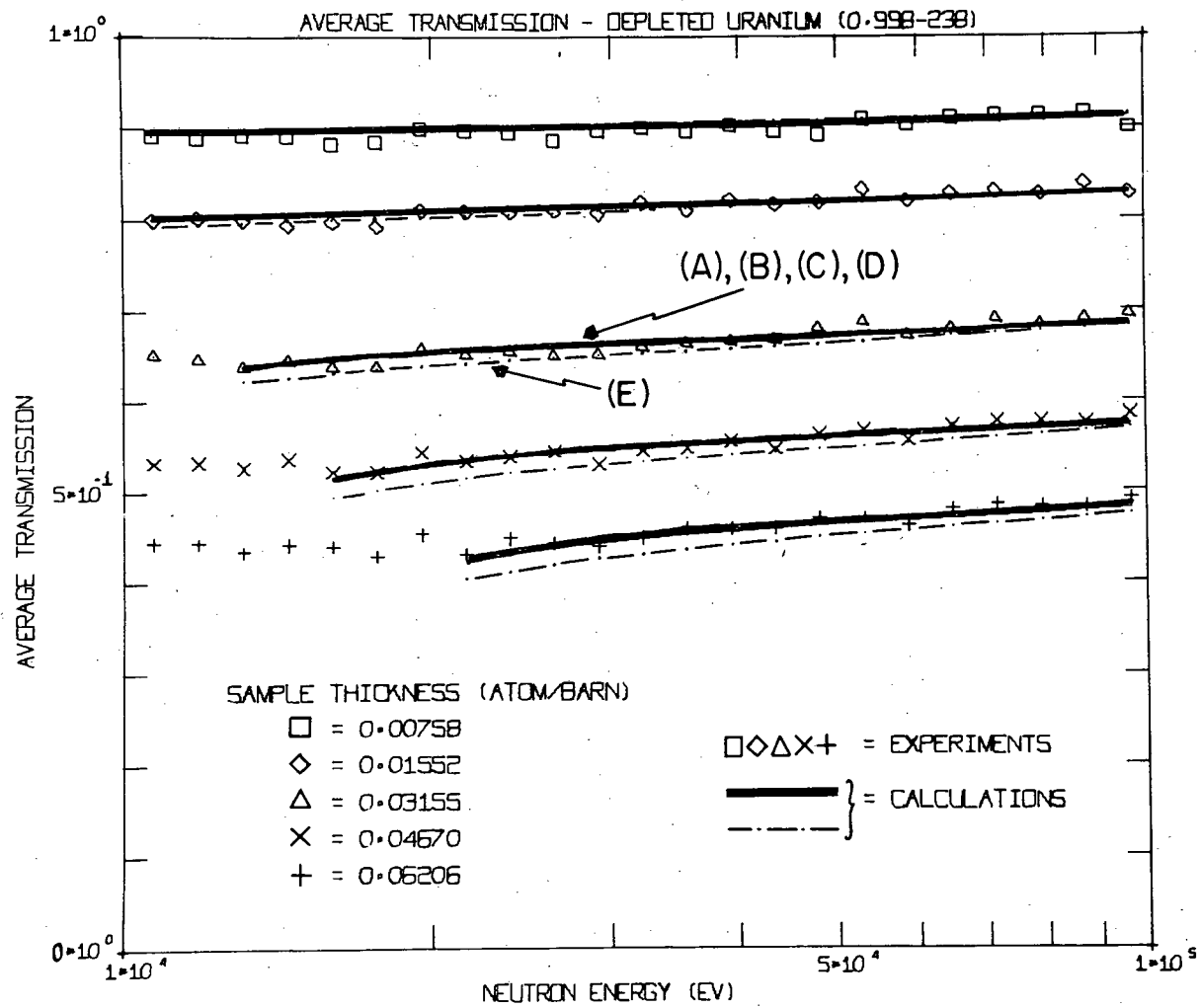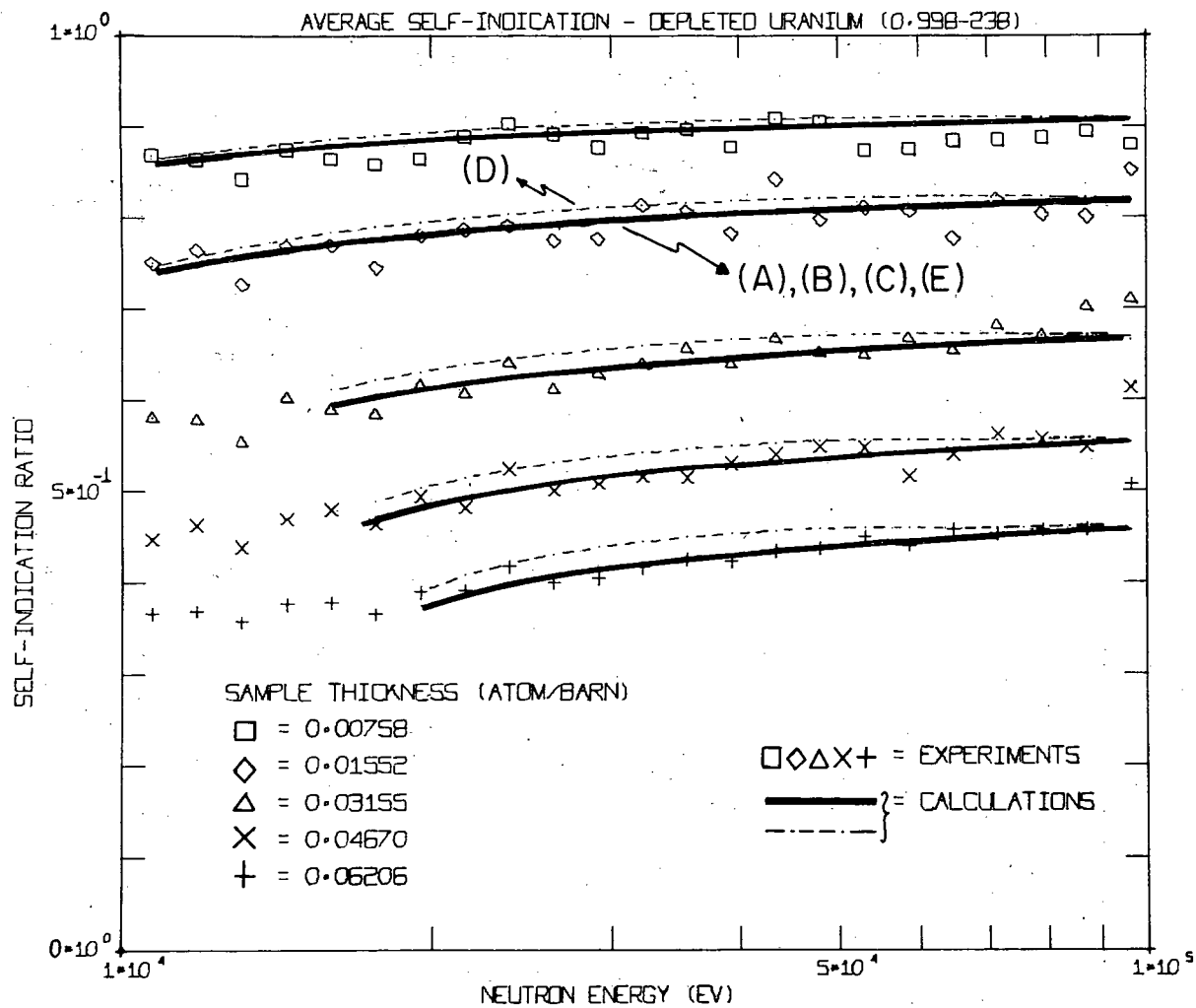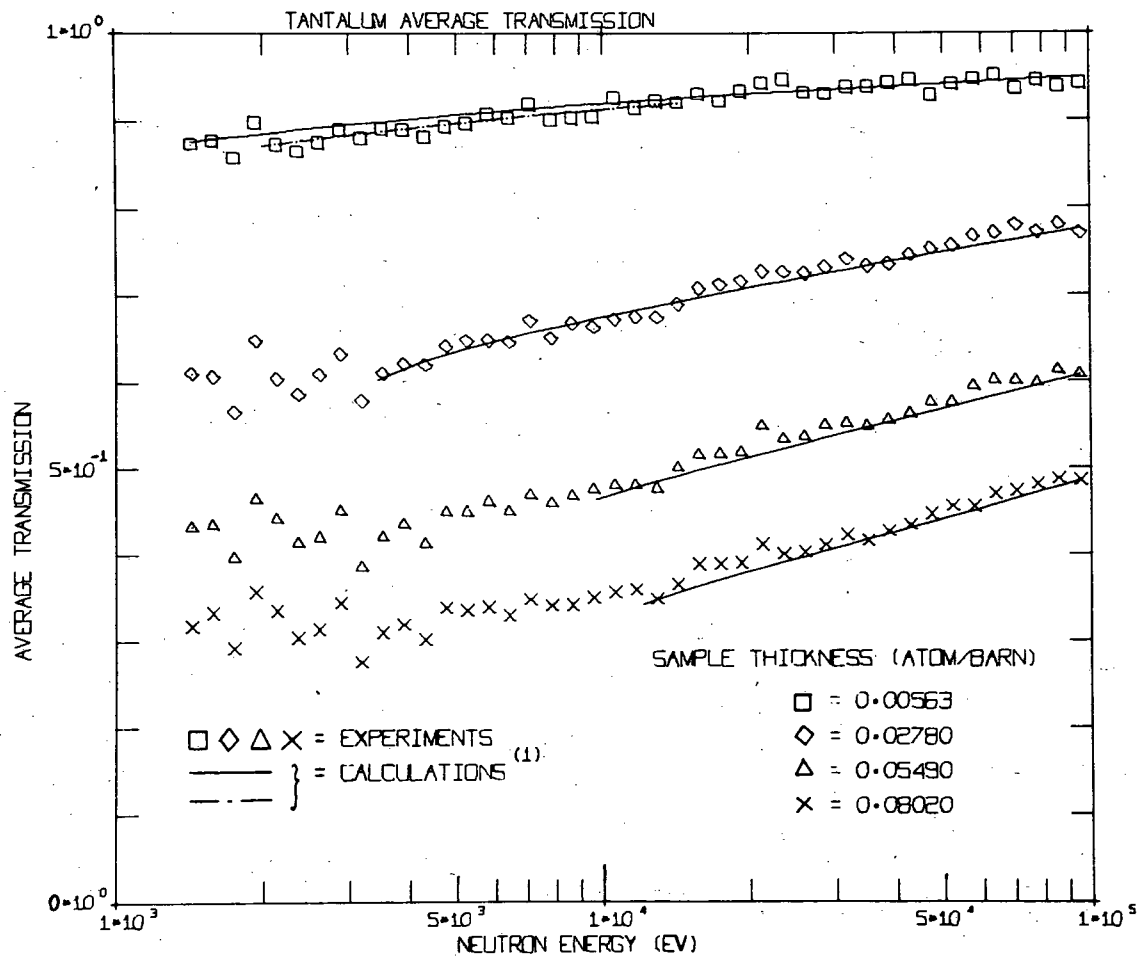
AVERAGE TRANSMISSION - DEPLETED URANIUM (0·998-238)

Figure 1a

Figure 1b

TANTALUM AVERAGE TRANSMISSION

AVERAGE TRANSMISSION

$1 \cdot 10^{0}$

$5 \cdot 10^{-1}$

$0 \cdot 10^{0}$

$1 \cdot 10^{3}$ $5 \cdot 10^{3}$ $1 \cdot 10^{4}$ $5 \cdot 10^{4}$ $1 \cdot 10^{5}$

NEUTRON ENERGY (EV)

SAMPLE THICKNESS (ATOM/BARN)

☐ = 0·00563
◇ = 0·02780
△ = 0·05490
✕ = 0·08020

☐ ◇ △ ✕ = EXPERIMENTS
——— } = CALCULATIONS (1)
—·—

(1) AVERAGE RESONANCE PARAMETERS:

——— $S_0 = 1.6 \times 10^{-4}$ } $S_1 = 0.4 \times 10^{-4}$, D_0 , $D_1 = 4.3$ and 2.15 (eV)
—·— $S_0 = 2.0 \times 10^{-4}$ } $\Gamma_{r_0}, \Gamma_{r_1}$ = 60.0 and 72 (mV), $R' = 8.19$ (fm)

Figure 2a

TANTALUM AVERAGE SELF-INDICATION RATIO

SAMPLE THICKNESS (ATOM/BARN)
☐ = 0·00563
◇ = 0·02780
△ = 0·05490
✕ = 0·08020

⎯⎯⎯
⎯·⎯ = CALCULATION (1)

☐◇△✕ = EXPERIMENTS

(1)

AVERAGE RESONANCE PARAMETERS:

⎯⎯ $S_o = 1.6 \times 10^{-4}$ ⎫ $S_1 = 0.4 \times 10^{-4}$, $D_o, D_1 = 4.3, 2.15$ (eV),

⎯·⎯ $S = 2.0 \times 10^{-4}$ ⎬ $\Gamma_{r_o}, \Gamma_{r_1} = 60, 72$ (mV), $R' = 8.19$ (fm)

Figure 2b

SENSITIVITY TO STRENGTH FUNCTIONS -- URANIUM-(SIR)

ENERGY RANGE   37.3 - 33.8 KEV
SAMPLE TEMPERATURE   293°K

■ ■   EXPERIMENTAL VALUES
───   BEST FIT PARAMETERS
─·─   DOUBLED P-WAVE STRENGTH
─··─   DOUBLED S- AND P-WAVE STRENGTH
─ ─   HALF OF S- AND P-WAVE STRENGTH

AVERAGE SELF-INDICATION-RATIO

SAMPLE THICKNESS (ATOM/BARN)

SENSITIVITY TO STRENGTH FUNCTIONS -- URANIUM-(TRANS)

ENERGY RANGE   37.3 - 33.8 KEV
SAMPLE TEMPERATURE   293°K

■ ■   BEST FIT PARAMETERS
─·─   DOUBLED P-WAVE STRENGTH
─··─   DOUBLED S- AND P-WAVE STRENGTH
─ ─   HALF OF S- AND P-WAVE STRENGTH

AVERAGE TRANSMISSION

SAMPLE THICKNESS (ATOM/BARN)

Figure 3

16

Figure 4

Table 1. Best Fit P-wave Strength Functions for ^{238}U for Different Scattering Lengths

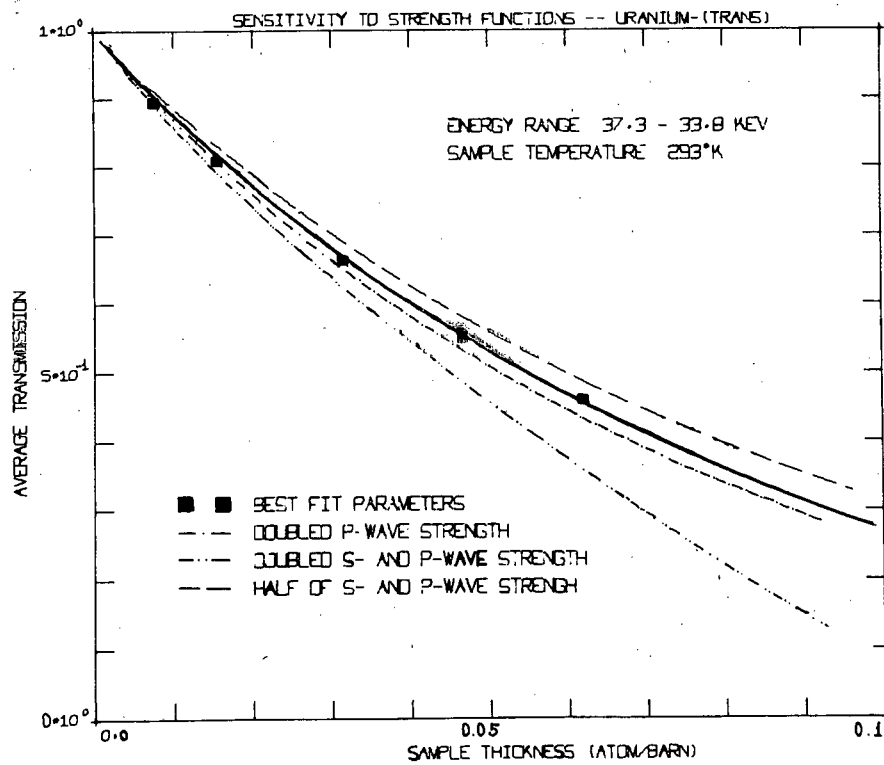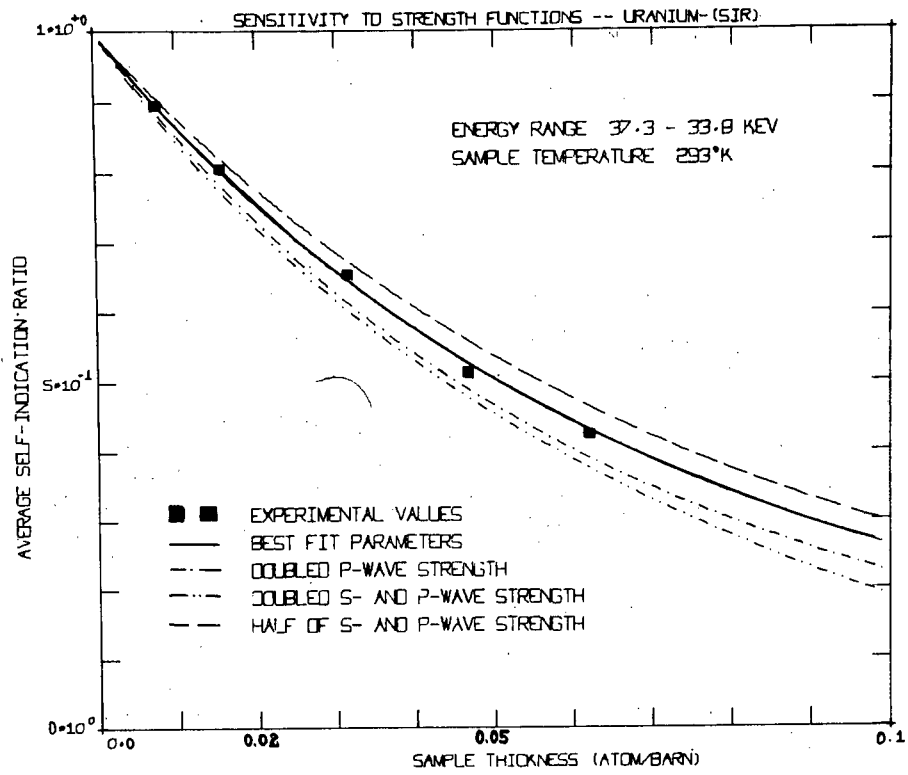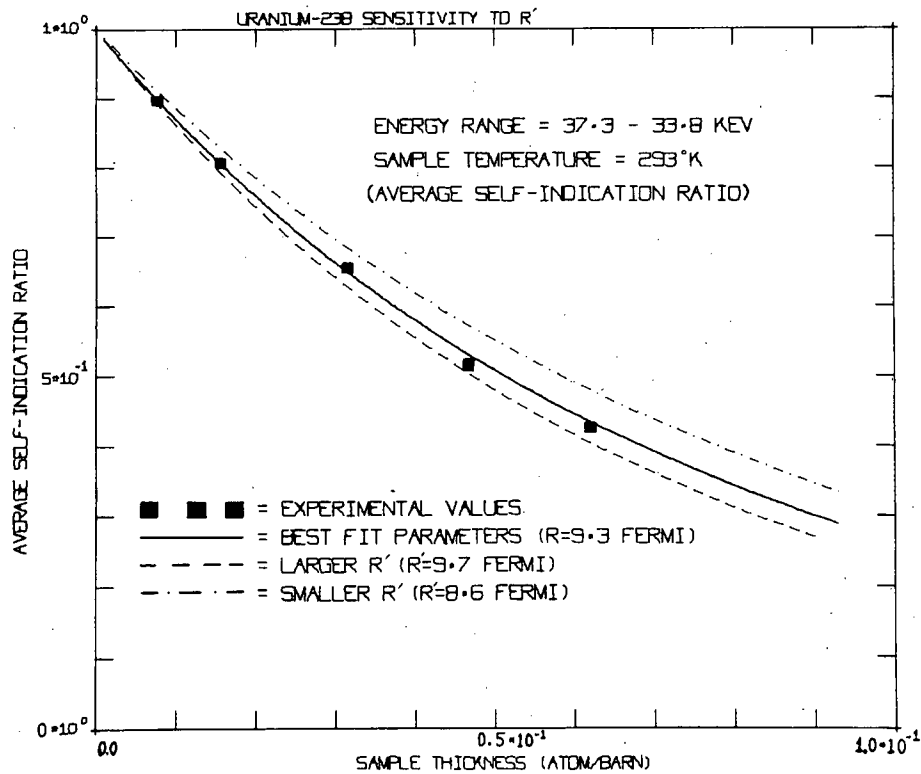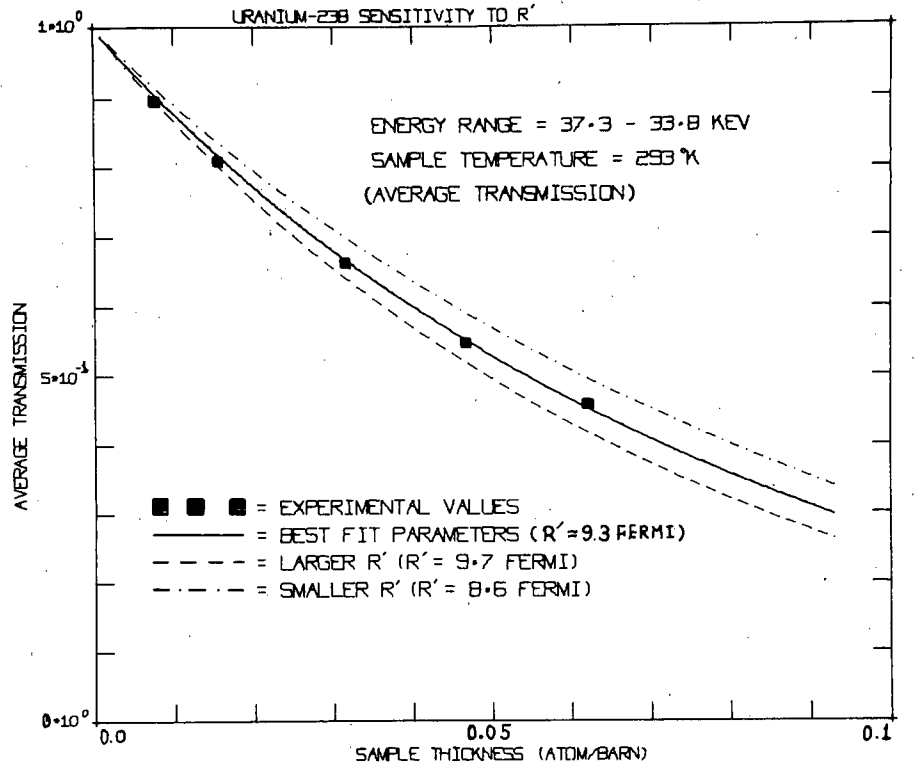| | Best Fit Parameters* | | | ENDF/B-III | |
	(A)	(B)	(C)	(D)	(E)#
$S_1(10^{-4})$	$1.58 \begin{smallmatrix} +0.1 \\ -0.1 \end{smallmatrix}$	$1.94 \begin{smallmatrix} +0.1 \\ -0.2 \end{smallmatrix}$	$2.40 \begin{smallmatrix} +0.1 \\ -0.2 \end{smallmatrix}$	1.75	1.27
$\langle D_1 \rangle$ (eV)	$11.3 \begin{smallmatrix} -2.0 \\ +2.0 \end{smallmatrix}$	$11.3 \begin{smallmatrix} -3.5 \\ +3.0 \end{smallmatrix}$	$11.3 \begin{smallmatrix} -2.0 \\ +3.0 \end{smallmatrix}$	6.67	6.90
$\overline{\Gamma}_{\gamma 1}$ (meV)	$47.5 \begin{smallmatrix} -8.4 \\ +8.4 \end{smallmatrix}$	$43.8 \begin{smallmatrix} -13.6 \\ +11.6 \end{smallmatrix}$	$37.0 \begin{smallmatrix} -6.6 \\ +9.8 \end{smallmatrix}$	23.5	28.0
R' (fm)	9.30	9.20	9.0	9.20	9.60
R (fm)	8.74	8.74	8.4	8.4	8.74
R^{∞}	− 0.065	− 0.053	− 0.071	− 0.095	−0.098
$S_0(10^{-4})$	1.0			1.05	1.0
$\langle D_0 \rangle$ (eV)	20.7			20.0	20.7
$\overline{\Gamma}_{\gamma 0}$ (meV)	23.0			23.5	23.0

*The uncertainties given for S_1, $\langle D_1 \rangle$, and $\overline{\Gamma}_{\gamma 1}$ correspond to the values which yield the average difference between the experimental values and theoretical values as follows:

$$\left| \overline{\Delta R} \right| = \left| \frac{1}{N} \sum_{i=1}^{N} (R_i^{exp} - R_i^{cal})/\delta R_i^{exp} \right| \leq 2.5$$

#R' = 9.60 fermi, taken from Columbia measurement[6]

Table 2. Best Fit Average Resonance Parameters of Tantalum
in the Energy Range from 10 to 100 keV

	S-wave ($\ell=0$)	P-wave ($\ell=1$)
Strength Function (10^{-4})	$1.6 \begin{smallmatrix} +0.3 \\ -0.2 \end{smallmatrix}$ *	$0.4 \begin{smallmatrix} -0.2 \\ +0.3 \end{smallmatrix}$
Level Spacing (eV)	$4.3 \begin{smallmatrix} -0.5 \\ +1.5 \end{smallmatrix}$	$2.15 \begin{smallmatrix} -0.25 \\ +0.75 \end{smallmatrix}$
Radiation Width (meV)	$60.0 \begin{smallmatrix} -5.0 \\ +3.5 \end{smallmatrix}$	$72.0 \begin{smallmatrix} -9.0 \\ +6.0 \end{smallmatrix}$
Scattering Length R' (fermi)	8.19 #	

*The error limitations given for all the parameters correspond
to the values which yield the average difference between the
experimental values and theoretical values as follows:

$$\left| \overline{\Delta R} \right| = \left| \frac{1}{N} \sum_{i=1}^{N} (R_i^{exp} - R_i^{cal})/\delta R_i^{exp} \right| \leq 2.5$$

#It is assumed that channel radius R is the same as R',
that is, $R^{\infty} = 0.0$.

CORRELATIONS BETWEEN REDUCED NEUTRON AND RADIATIVE WIDTHS
IN NEUTRON RESONANCES

M. Lubert,[*] R. C. Block and N. C. Francis

The cross section measurements conducted at the RPI LINAC
with the chromium and nickel isotopes showed strong correlations
between the reduced neutron and total radiative widths.[1] Further,
the ^{60}Ni capture cross section below the 12.4 keV resonance dis-
played a significant slowly varying cross section of approximately
50 mb.

These phenomena were investigated with a capture model which
includes both channel and compound contributions to the cross
section. This is similar to the nuclear model formulated by
Lane and Lynn.[2] The nuclear reaction model is one of an s-wave
neutron coupled to the core of the target nucleus which undergoes
an El transition to a low-lying single particle state without
forming a compound nucleus. The theory was developed in terms of
R-matrix theory by considering the external region of configura-
tion space to coincide with the channel region. The dipole matrix
element was evaluated using R-matrix phase shifts to define the
final continuum states. The resonance parameters were consistent
with the neutron total cross section measurements at RPI.[1] The
basic partial radiative width data for ^{53}Cr and ^{61}Ni was obtained
from the photothreshold experiments of Baglan[3] and Jackson.[4]

^{53}Cr (γ,n) Analysis

The 3/2$^-$ ground state makes a transition to the $\frac{1}{2}^+$ final
positive energy neutron state. The neutron reduced width for the
^{53}Cr lowest energy bound state was obtained by fitting the line
shape reported by Jackson below the 92 keV level. The reduced
width factor, $\theta_o^2 = 0.35$, for the ^{53}Cr target nucleus bound state
was derived with the single particle state normalized to unity
for the region outside the nuclear surface. The partial channel

---

[*]Based in part on the Ph.D. Thesis of M. Lubert.

radiative width, $\Gamma_{\gamma 0}^{ch}$, for each resonance was calculated from the theoretical channel cross section. The experimental partial widths, $\Gamma_{\gamma 0}$, were obtained by adding the channel and compound nucleus amplitudes and squaring.

$$\Gamma_{\gamma 0} = (\sqrt{\Gamma_{\gamma 0}^{ch}} + \sqrt{\Gamma_{\gamma 0}^{cn}})^2$$

$\Gamma_{\gamma 0}^{cn}$ is the partial compound nucleus width which is obtained from this equation. The thermal neutron capture cross section of ^{52}Cr for ground state transitions was obtained from the (γ,n) analysis using detailed balance. The experimental thermal (n,γ) cross section was multiplied by a measured ground state branching ratio[5] to yield 0.55b. The theoretical value was 0.53b. Negative energy state compound nucleus contributions were neglected in view of the fact that none were necessary for the total cross section calculation. In addition, the 50.2 keV resonance compound nucleus contribution to the ground state does not add significantly to the thermal (n,γ) cross section.

As a further test of the model and its parameters, the calculated total radiative widths for the 50.2 and 97.1 keV resonances were compared to experiment.[1] The theoretical total widths were obtained from the separate channel and compound nucleus components. The channel-compound nucleus interference part was neglected since their sum is expected to be small due to the random sign of the compound nucleus amplitude. The ground state channel capture width was determined from the ^{53}Cr(γ,n) calculation. The total channel capture width was determined using the thermal neutron ground state transition branching ratio. The compound nucleus part of the cross section for the excited state transitions was estimated by using the average compound nucleus width from the ^{53}Cr (γ,n) analysis. The photon energy cubed dipole law was assumed. The measured Γ_{γ}^{exp} and calculated widths $\Gamma_{\gamma}^{cal'd}$ are shown in Table 1.

Table 1. Calculated and Measured ^{52}Cr Total Radiative Widths

E_o(keV)	Γ_γ^{exp}(eV)	$\Gamma_\gamma^{cal'd}$(eV)
50.2	1.16	1.49
97.1	4.80	3.70

^{61}Ni Analysis

Similar results have been obtained for the ^{61}Ni (γ,n) and the ^{60}Ni (n,γ) reactions. The reduced width, $\theta_o^2 = 0.17$, was obtained from fitting Jackson's experimental data. These are summarized in Table 2.

Table 2. Calculated and Measured ^{60}Ni Total Radiative Widths

E_o(keV)	Γ_γ^{exp}(eV)	$\Gamma_\gamma^{cal'd}$(eV)
12.5	3.3	3.6
28.6	1.6	1.1

The calculated thermal ^{60}Ni (n,γ) cross section of 1.2b compares well with the 1.1b reported in BNL-325. The RPI measurements for ^{60}Ni (n,γ) reported an asymmetry in the 12.5 keV line shape. The measured cross section, which exhibits constructive interference below the resonance, is 50 mb at about 5 keV. The calculated cross section displays a similar line shape and a cross section of 20 mb at 5 keV.

The analysis of the (n,γ) and (γ,n) experiments indicate: (1) The absence of (γ,n) experimental correlations between the $\Gamma_{\gamma o}$ and Γ_n^o is due to two factors. First, this correlation is reduced by the random compound nucleus partial radiative amplitude which adds coherently to the channel amplitude. Second, the experimental correlation may be reduced because of experimental error. The (γ,n) experiments are difficult to perform and subject to area and background uncertainties; (2) The correlations ob-

served at RPI between the reduced neutron and total radiative widths for the nickel and chromium isotopes can be interpreted as due to correlations between partial radiative and reduced neutron widths for several final states where the interference between the channel and compound nucleus has cancelled. This indicates non-statistical effects such as channel capture are important in the radiative process; (3) The resonance line shapes determined by the theory are asymmetric. This characteristic shape is expected when the channel width is greater than the compound nucleus contribution; (4) If one has measured the partial cross section to some final state for an isotope, this analysis can determine the reduced width. This provides another method, besides the (d,p) reaction, for calculating the reduced width; (5) The channel cross section shapes differ from the Breit-Wigner theory. In particular, the channel cross section below the resonance energy is greater than the Breit-Wigner cross section. As neutrons diffuse through materials such as iron, the neutron flux is depressed at the resonance and is large at the total cross section minima positions. At these latter energies, the difference between the channel and compound nucleus cross section is large and the channel reaction rate can be significant.

REFERENCES:
1. R. G. Stieglitz et al., Nucl. Phys., A163, 592 (1971).
2. A. M. Lane, J. E. Lynn, Nucl. Phys., 17, 586 (1960).
3. R. J. Baglan, Ph.D. Thesis, UCRL-50902 (August 1970).
4. H. E. Jackson, E. N. Strait, Phys. Rev., C4, 1314 (1971).
5. B. J. Allen et al, AAEC E200 (October 1969).

ANGULAR MOMENTUM DEPENDENT OPTICAL MODEL FOR NONSPHERICAL NUCLEI

P. J. Turinsky and Jose' Sierra[*]

To simultaneously fit experimental data on the s- and p-wave strength functions and potential scattering radii for low energy neutrons versus mass number, an angular momentum dependent spherical optical model was found necessary.[1] By introducing an angular momentum dependent imaginary surface potential, excellent fits were obtained to the strength functions deep minima and maxima and also the oscillatory potential scattering radius in the mass number region of strongly spherical nuclei. For mass numbers greater than 140, low lying 2^+ rotator states require the use of a nonspherical optical potential via coupled-channel calculations.

Employing our angular momentum dependent spherical optical model parameters, coupled-channel calculations allowing 0^+-2^+ vibrator state coupling were carried out using the JUPITØR program. Deformation parameters β_2+ and excitation energies E_2+ were obtained for various isotopes from their E2 transition data,[2] hence no new parameters had to be determined. Figure 1 illustrates the improved agreement between experiment and calculation in the mass number region of the s-wave strength function splitting due to 0^+-2^+ vibrator state coupling. An excellent fit to the p-wave strength function data about the deep minima at mass number 170 is shown in Fig. 2. Both the sharp p-wave strength function resonance about mass number 224 and more oscillatory potential scattering radii predicted as shown in Fig. 3, cannot be substantiated for lack of experimental data.

Neutron total, shape-elastic and reaction cross sections versus target mass number and incident neutron energy have also been calculated using our angular momentum dependent optical model in coupled-channel calculations. Figure 4 contrasts the

---

[*]Based in part on the Master of Science Thesis of Jose' Sierra.

neutron total cross section at 100 keV as obtained experimentally and from Perey-Buck's[3] spherical and our optical model with and without vibrator states treated. With the considerable variation of the total cross section from isotope to isotope, neither optical model is capable of exact predictions over the mass number range 40-240. It does appear that our angular momentum dependent spherical optical model is preferred over Perey-Buck's spherical optical model; likewise, our angular momentum dependent optical model treating rotator states is most highly preferred. Prediction capability problems are noted in the total cross section maxima, but as Fig. 5 illustrates, this problem arises since severe energy sensitivity exists at maxima due to the "just" single-particle binding effect.

With fission product productions peaking in the mass regions 90-100 and 130-140, Figs. 4-5 illustrate the considerable difficulty one encounters in predicting fission product cross section behavior due to the strong mass number and energy dependence in these mass ranges. However, when confronted with a lack of experimental cross section information (as required in reactor physics calculations) in these mass number ranges, the angular momentum dependent optical model with vibrator state coupling appears the preferred prediction model to employ.

REFERENCES:

1. Linear Accelerator Project Annual Technical Report, October 1, 1971 - September 30, 1972, 63, COO-3058-27.

2. Nuclear Data, Section A, K. Way, Ed., pp 29-34, Academic Press, New York (1965).

3. B. Buck and F. Perey, Phys. Rev. Letters, 8, 444 (1962).

FIGURE CAPTIONS

Fig. 1   Neutron s-wave Strength Function Versus Mass Number at
         100 keV.

Fig. 2   Neutron p-wave Strength Function Versus Mass Number at
         100 keV.

Fig. 3   Neutron Potential Scattering Radius Versus Mass Number at
         100 keV.

Fig. 4   Neutron Total Cross Section Versus Mass Number at 100 keV
         as   obtained   from Experimental Data and Various Prediction
         Models.

Fig. 5   Neutron Total Cross Section Versus Mass Number at 30 keV
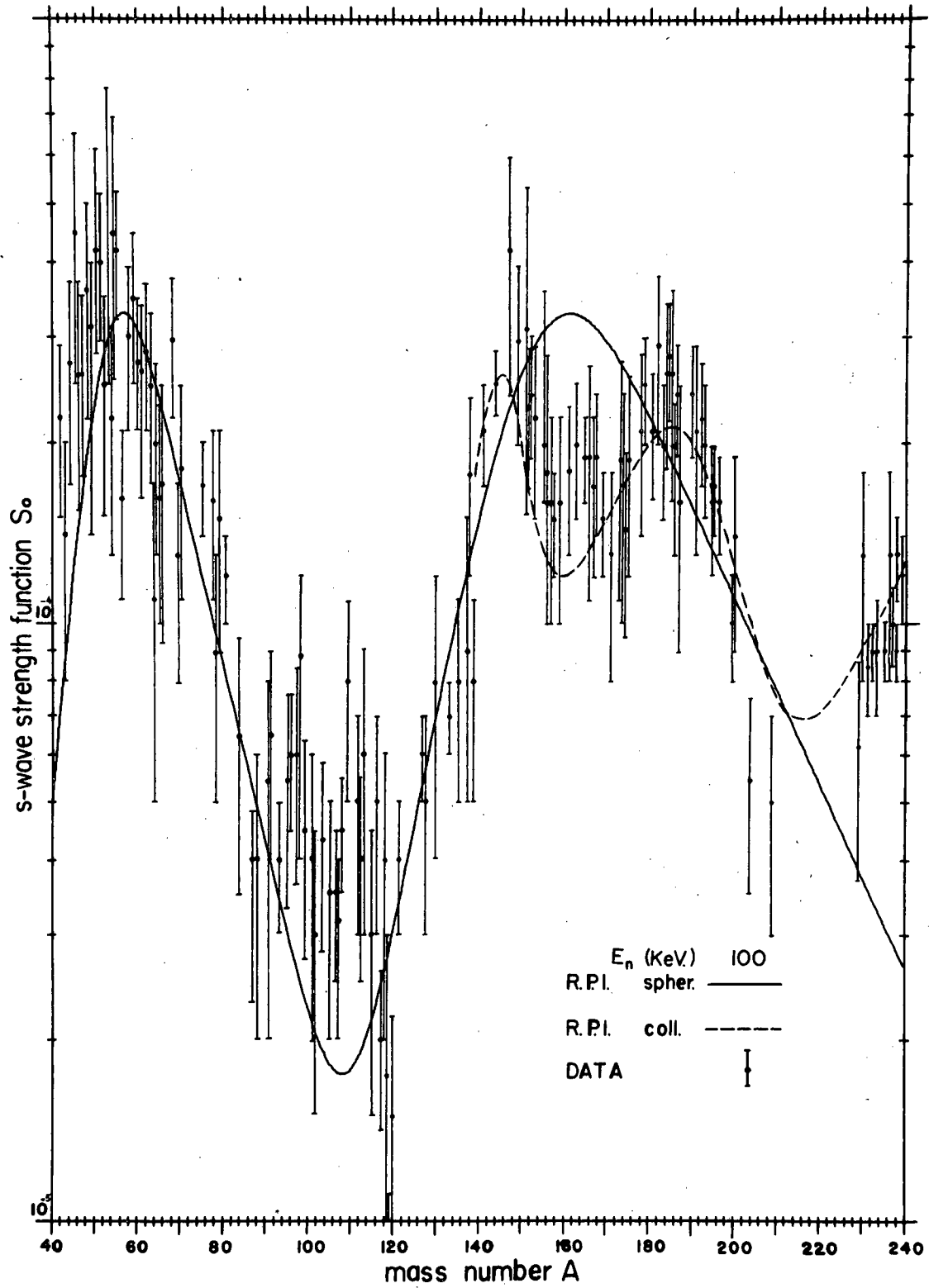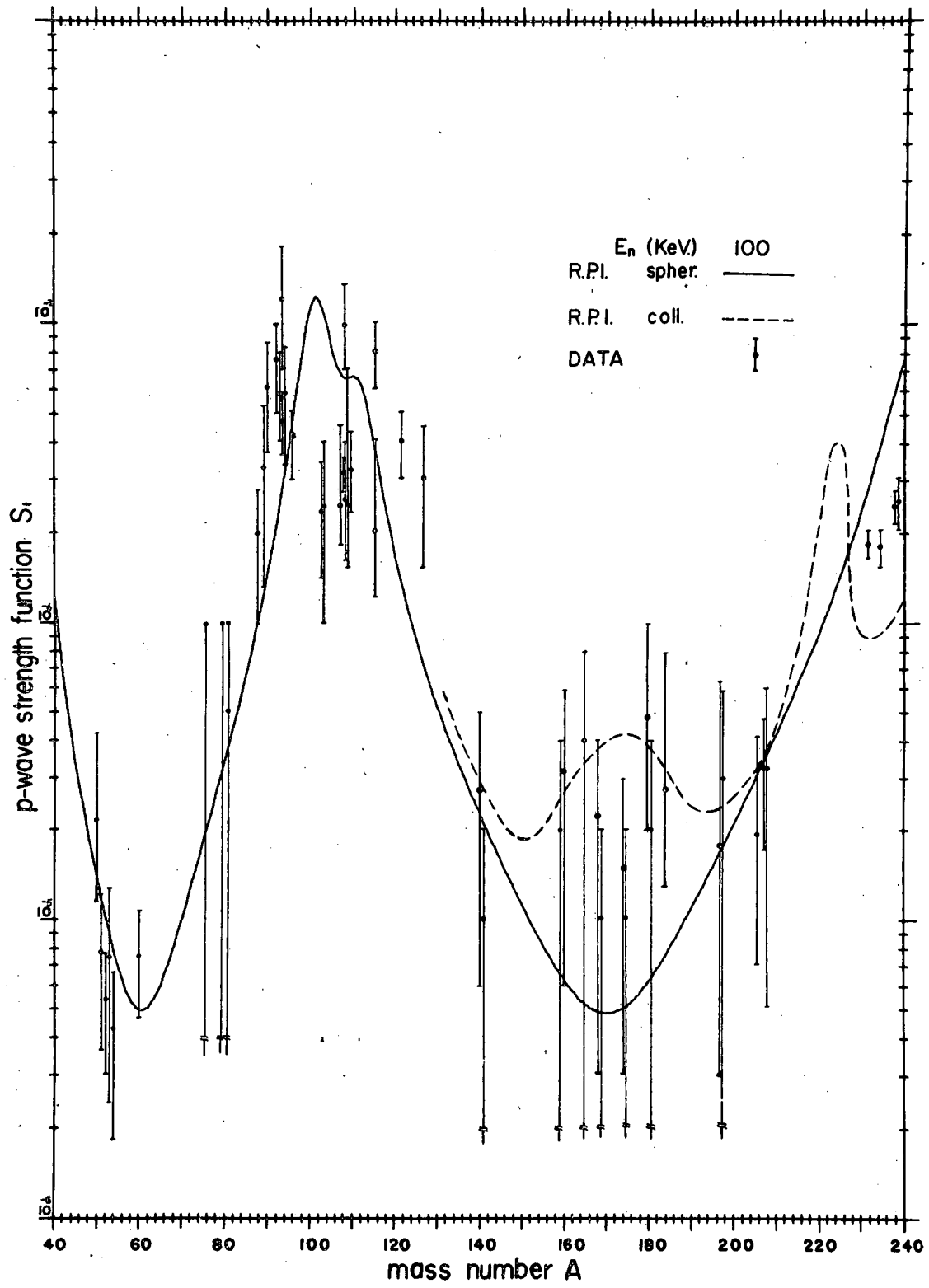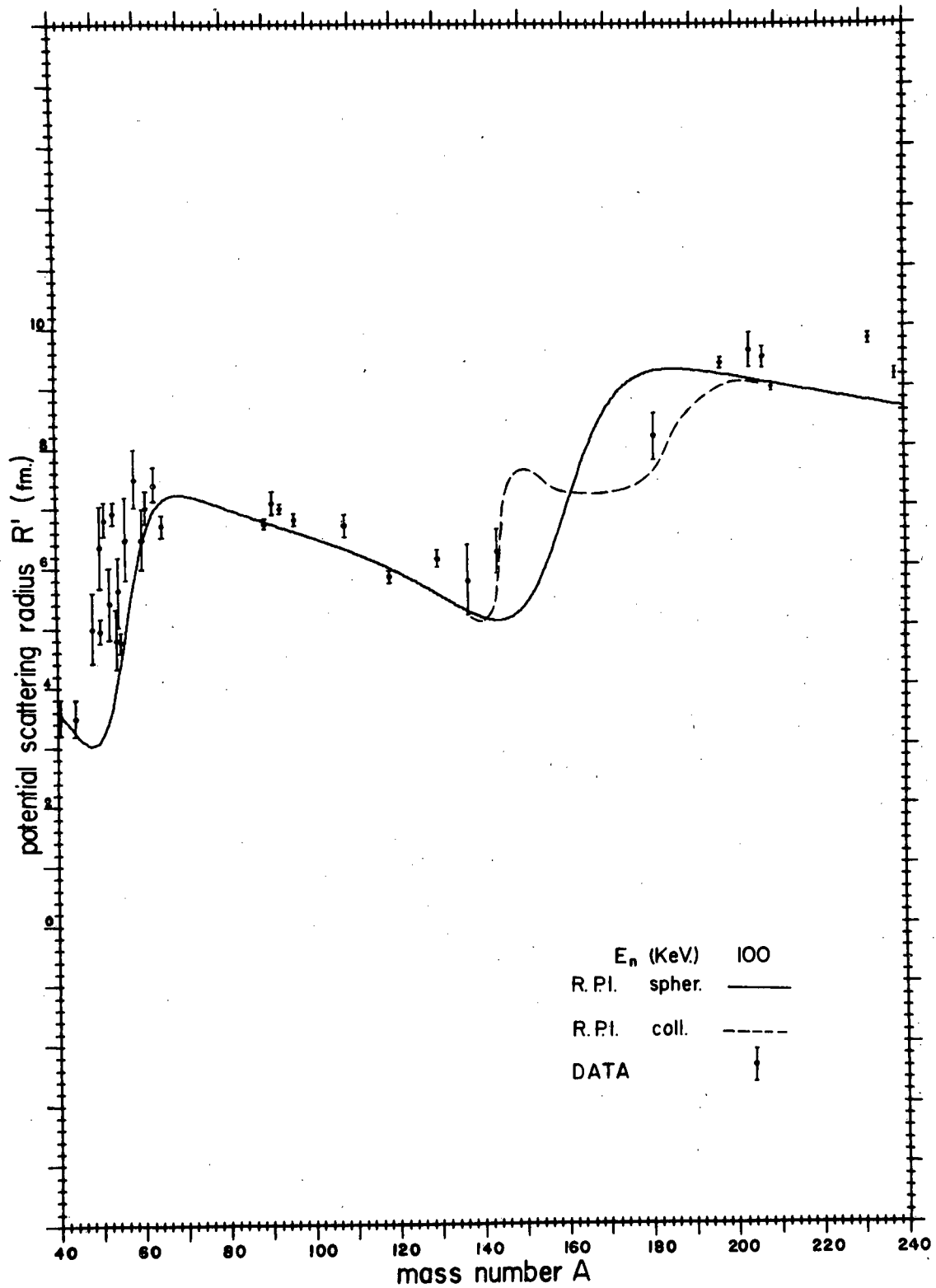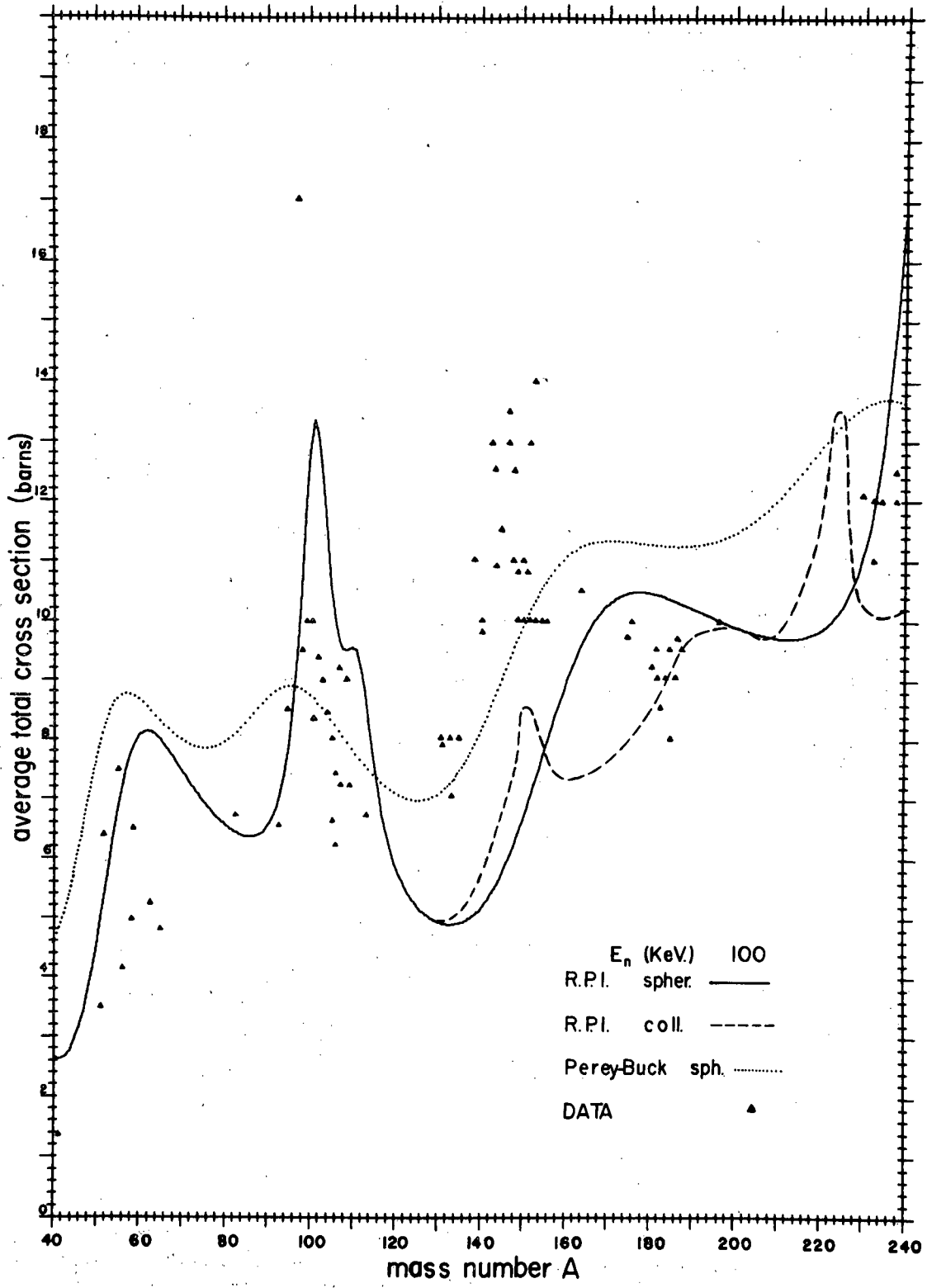   and 100 keV Illustrating Energy Sensitivity of Maxima.

Figure 1

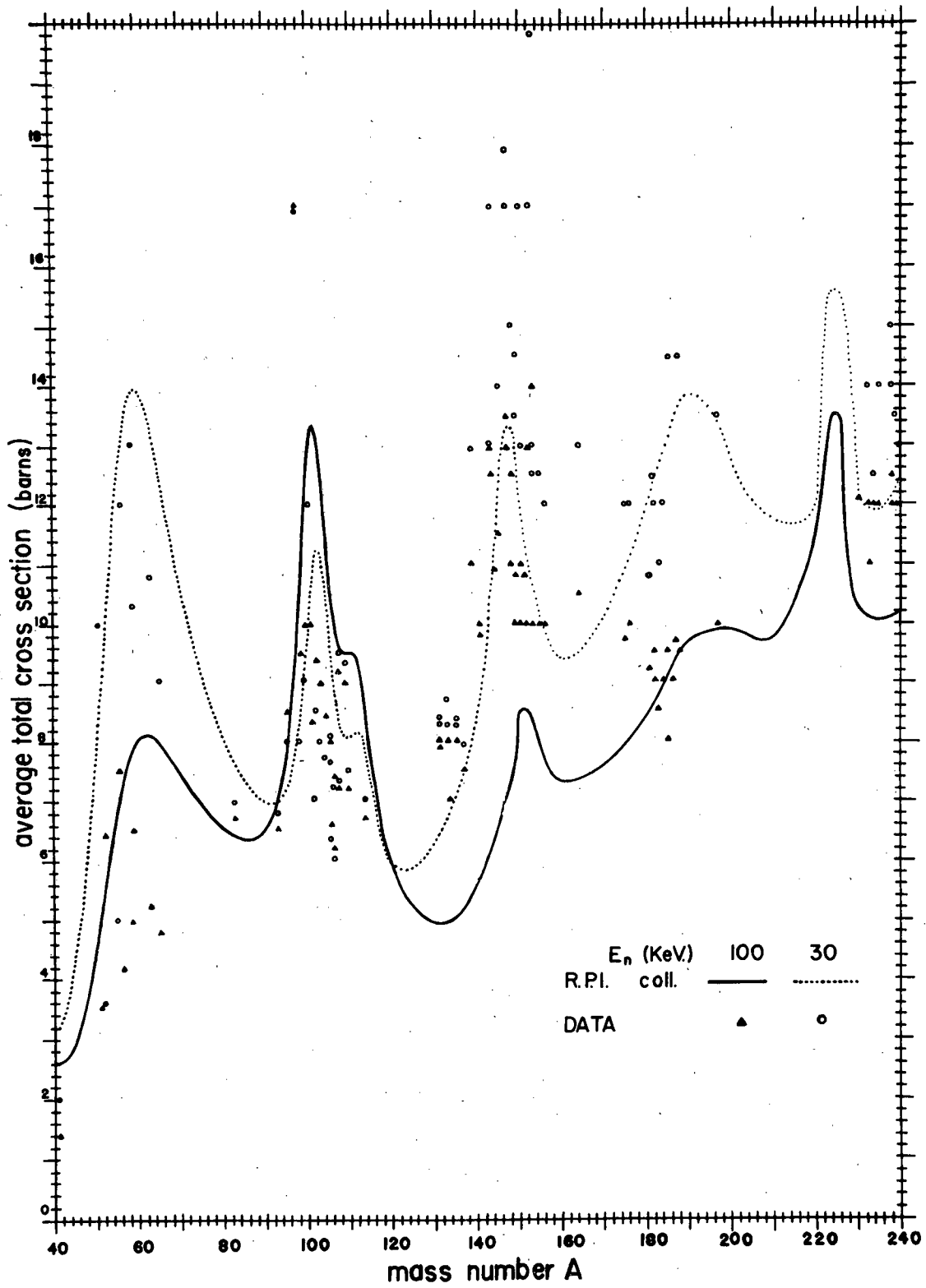Figure 2

Figure 3

Figure 4

Figure 5

PSEUDO THREE PARTICLE CALCULATIONS INVESTIGATING
THE FOUNDATIONS OF THE OPTICAL MODEL

J. Sierra[*] and P. J. Turinsky

As previously reported,[1] to simultaneously fit experimental values of the s- and p-wave strength functions and potential scattering radii for low energy neutrons versus mass number (A) by optical model calculations, an angular momentum (ℓ) surface imaginary potential (W_ℓ) was required. Theoretical justification of this potential form has been undertaken by considering a pseudo three particle scattering system where the target nucleus with A nucleons is modeled as an inert core of (A-1) spinless nucleons (Particle [1]) and a bound nucleon (Particle [2]) which can be excited by the incident neutron (Particle [3]). A 2p-1h basis is therefore used, with the system Hamiltonian modeled by

$$H = \frac{P_1^2}{2M_1} + \frac{P_2^2}{2M_2} + \frac{P_3^2}{2M_3} + V_{SM}(|\vec{r}_1-\vec{r}_2|) + V_{SM}(|\vec{r}_1-\vec{r}_3|) + V_{pp}\delta(\vec{r}_2-\vec{r}_3)$$

(1)

where V_{SM} indicates the real, central shell model potential with spin orbit force. Equation (1) indicates that the (A-1) nucleons exert a shell model potential on the bound nucleon and incident neutron; whereas, the latter two particles interaction is a point interaction for calculational simplicity. Changing to the center-of-mass coordinate system and restricting $M_1 \gg M_2$ or M_3, we obtain the two particle relative Hamiltonian

$$H_{Rel} = \frac{p^2_{\zeta_2}}{2M_2} + \frac{p^2_{\zeta_3}}{2M_3} + V_{SM}(|\vec{\zeta}_2|) + V_{SM}(|\vec{\zeta}_3|) + V_{pp}\delta(\vec{\zeta}_2-\vec{\zeta}_3) \qquad (2)$$

---

[*]Based in part on the Master of Science Thesis of Jose' Sierra.

where $\vec{\zeta}_2 = \vec{r}_1 - \vec{r}_2$ and $\vec{\zeta}_3 = \vec{r}_1 - \vec{r}_3$. The related Hamiltonian equation

$$H_{Rel}[\Psi] = E\Psi(\vec{\zeta}_2, \vec{\zeta}_3) \tag{3}$$

is solved by expanding $\Psi(\vec{\zeta}_2, \vec{\zeta}_3)$ as

$$\Psi^{J^\pi}(\vec{\zeta}_2, \vec{\zeta}_3) = \sum_c \frac{U_c^{J^\pi}(|\vec{\zeta}_3|)}{|\vec{\zeta}_3|} \left(\varphi_{\ell_3 j_3} \otimes \Psi_{\ell_2 j_2 n_2}\right)_{J^\pi} \tag{4}$$

with $\otimes$ indicating angular momentum coupling to total angular momentum J with parity π and $c = (\ell_3 j_3 \ell_2 j_2 n_2)$. Denoting the spherical harmonics as $Y_\ell^m(\theta, \varphi)$ and spin ($\frac{1}{2}$) vectors as $X_s^{m_s}$, we define

$$\varphi_{\ell_i j_i m_{j_i}} = \left(Y_{\ell_i}^{m_{\ell_i}} \otimes X_{s_i}^{m_{s_i}}\right)_{j_i m_{j_i}} . \tag{5}$$

The wave function $\Psi_{\ell_2 j_2 m_{j_2} n_2}$ represents the single bound particle

and is obtained by solving the shell model Hamiltonian equation

$$\left[\frac{p_{\zeta_2}^2}{2M_2} + V_{SM}(|\vec{\zeta}_2|)\right][\Psi_{\ell_2 j_2 m_{j_2} n_2}] = E_{n_2}^{\ell_2 j_2} \Psi_{\ell_2 j_2 m_{j_2} n_2} \tag{6}$$

where the decomposition

$$\Psi(\vec{\zeta}_2)_{\ell_2 j_2 m_{j_2} n_2} = W(|\vec{\zeta}_2|)_{\ell_2 j_2 n_2} \varphi_{\ell_2 j_2 m_{j_2}} \tag{7}$$

is employed. Using Eqs. (3-6) in Eq. (2) leads to the coupled-channel equations for $U_c^{J^\pi}(|\vec{\zeta}_3|)$

$$\frac{-\hbar^2}{2M_3} \frac{d^2 U_c^{J\pi}}{d\zeta_3{}^2} + \left\{ V_{SM}(|\vec{\zeta}_3|) + \frac{\ell_3(\ell_3+1)\hbar^2}{2M_3\zeta_3{}^2} \right\} U_c^{J\pi}$$

$$+ \sum_{c'} < \varphi_{\ell_3 j_3} \otimes \Psi_{\ell_2 j_2 n_2})_{J\pi} |V_{pp}\delta(\vec{\zeta}_2 - \vec{\zeta}_3)| (\varphi_{\ell_3' j_3'} \otimes \Psi_{\ell_2' j_2' n_2'})_{J\pi} > U_{c'}^{J\pi}$$

$$\text{(8)}$$

$$= (E - E_{n_2}^{\ell_2 j_2}) \; U_c^{J\pi} \; .$$

Realizing that the optical model equation is identical to Eq. (8) when $(\ell_2 j_2 n_2)$ is equivalent to the unperturbed bound particle state, this implies that the complex optical potential must be expressed by

$$V_{Opt}(|\vec{\zeta}_3|) = \left[\sum_{c'} < (\varphi_{\ell_3 j_3} \otimes \Psi_{\ell_2 j_2 n_2})_{J\pi} |V_{pp}\delta(\vec{\zeta}_2 - \vec{\zeta}_3)| (\varphi_{\ell_3' j_3'} \otimes \Psi_{\ell_2' j_2' n_2'})_{J\pi} > U_{c'}^{J\pi} / U_c^{J\pi} \right.$$

$$\text{(9)}$$

$$\left. + V_{SM}(|\vec{\zeta}_3|) \right]$$

By assuming the point interaction, the coupling potential in Eqs. (8) and (9) can be analytically evaluated avoiding all integrations. If Eq. (8) is solved for $\left\{ U_{c'}^{J\pi} \right\}$ with appropriate scattering boundary conditions, an estimate of V_{Opt} is obtained from Eq. (9). Do note that Eq. (9) indicates the optical potential to contain $(J^\pi \ell_3 j_3)$ dependence. Weak J^π dependence is hoped for since our currently used form which fits the experimental data has no J^π dependence.

The coupling potentials have been evaluated by choosing the last bound particle as the excitable nucleon and adjusting the parameters of V_{SM} to correctly bind this particle for a given mass number. These parameters were determined by using the ABACUS code in the bound state mode, thus also calculating

$\left\{ W(|\vec{\zeta}_2|) \right\}_{\ell_2 j_2 m_2}$ needed in the coupling potential evaluation. The numerical

solution of Eq. (8) is presently underway.

REFERENCE:

1. Linear Accelerator Project Annual Technical Report, October 1, 1971 - September 30, 1972, 63, COO-3058-27.

REACTOR PHYSICS AND ENGINEERING - EXPERIMENTAL

21,854

FAST AND INTERMEDIATE NEUTRON SPECTRUM MEASUREMENTS
IN A BULK SODIUM ASSEMBLY

A. N. Mallen,[*] N. N. Kaushal, B. K. Malaviya and E. R. Gaerttner

Measurements of neutron spectra have been made in a bulk
sodium assembly, of which a schematic diagram is shown in Fig. 1,
for radii of 10.5, 18.5, 26.5 and 34.5 inches from the source.
Two separate neutron sources were used during the course of these
experiments. The first was an air-cooled Ta-Pb target[1,2] and
the second was an oil-cooled Ta-Pb target[3] capable of handling
large (5000 watts) linac beam powers. The spectrum of the oil-
cooled target is significantly different from the spectrum of the
air-cooled target. This necessitates separate calculational
analyses of the data taken with the two different targets. The
introduction of the high power oil-cooled target in the sodium was
necessary, despite the additional effort required for analysis,
because of low neutron intensities encountered with the low power
air-cooled target. Additionally, the oil-cooled target provides
a large increase in low energy neutrons (due to slowing down in
the hydrogenous coolant), thus permitting a more thorough exam-
ination of the principal sodium resonance at 2.85 keV, and extend-
ing the range of fast spectra measurements downward in energy
from 10 keV to 10 eV.

Preliminary calculations have been performed using the one-
dimensional SN Code DTF-IV[4] for the air-cooled target, using
49 groups in the energy range 10 keV to 10 MeV, P_8 scattering,
the black absorber model[5] and using ENDF/B-3 data. Figures 2, 3
and 4 show some comparisons of measured spectra in the forward
direction ($\theta = 0°$, $\mu = 1.0$), with calculated spectra (the super-
posed histograms) using a P_{15} asymmetric quadrature
($\theta = 3° 20'$, $\mu = .99831$).

The calculation and experiment were both normalized to the
source spectrum. As can be seen from the figures, the calcula-
tion and experiment agree quite well for Hole 1, 25.5" deep

(R = 10.5"), and Hole 1, 17.5" deep (R = 18.5"), but deviates significantly from Hole 1, 9.5" deep (R = 26.5") most noticeably at high energies, where the fast flux is underpredicted by as much as a factor of 2.

Further measurements (with the new oil-cooled target) and calculations extending down to much lower energies (about 10 eV) are necessary for meaningful checks of sodium cross-section data. Such measurements and analyses are continuing.

REFERENCES:

1. B. K. Malaviya, E. Greenspan and E. R. Gaerttner, "Development of Special Targets for Fast Neutron Spectrum Studies," Trans. Am. Nucl. Soc., 11, 24 (1968).

2. Linear Accelerator Project Annual Technical Report, October 1, 1970 - September 30, 1971, 113, COO-3058-1.

3. Linear Accelerator Project Annual Technical Report, October 1, 1971 - September 30, 1972, 89, COO-3058-27.

4. K. D. Lathrop, "DTF-IV - A Fortran IV Program for Solving the Multi-group Transport Equation with Anisotropic Scattering," Los Alamos Scientific Laboratory (1965).

5. Linear Accelerator Project Progress Report, October - December 1969, 19, RPI-328-173.

FIGURE CAPTIONS

Fig. 1   Schematic Diagram of the Sodium Assembly

Figs. 2-4   Comparison of Measured Spectra Using the Air-cooled Ta-Pb Target, with Calculated Spectra (49 groups, P_8 scattering, P_{15} asymmetric quadrature, 'black absorber' one-dimensional model). Source normalized.

(2) Hole 1, 25.5" deep (R = 10.5", μ = 1.0)

(3) Hole 1, 17.5" deep (R = 18.5", μ = 1.0)

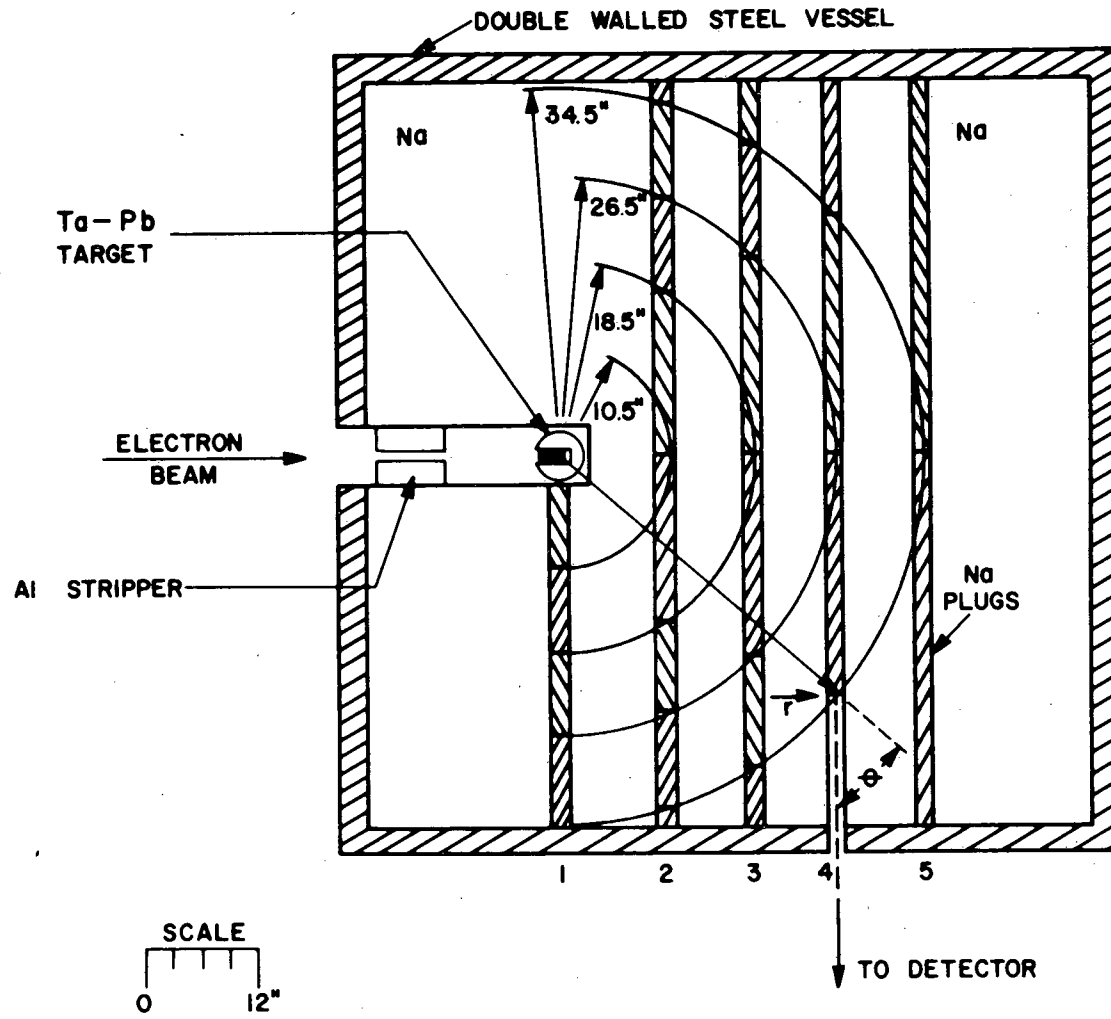(4) Hole 1, 9.5" deep (R = 26.5", μ = 1.0)
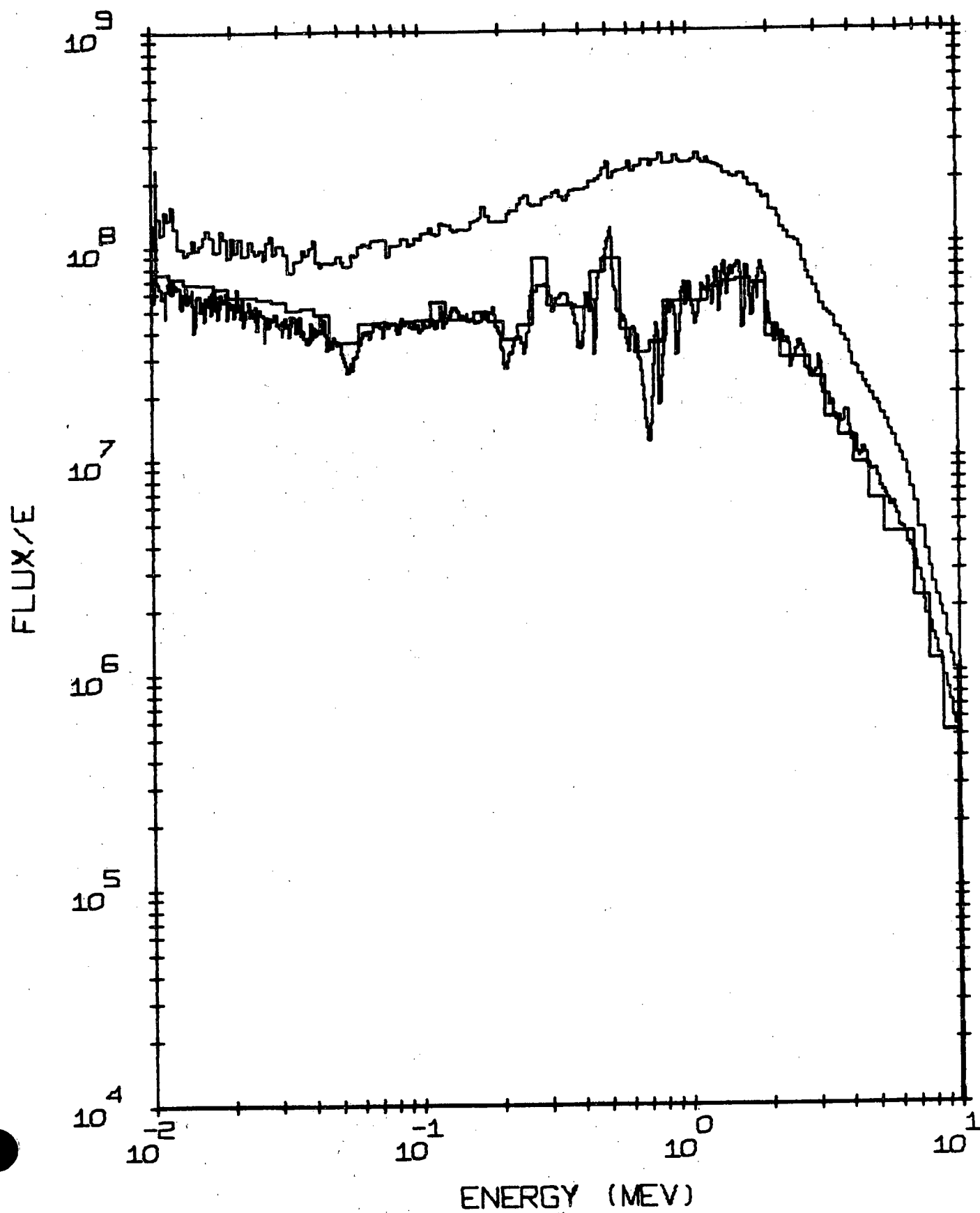
SODIUM ASSEMBLY

Figure 1

SOURCE, AND R=10.5 IN, MU=1.00

Figure 2

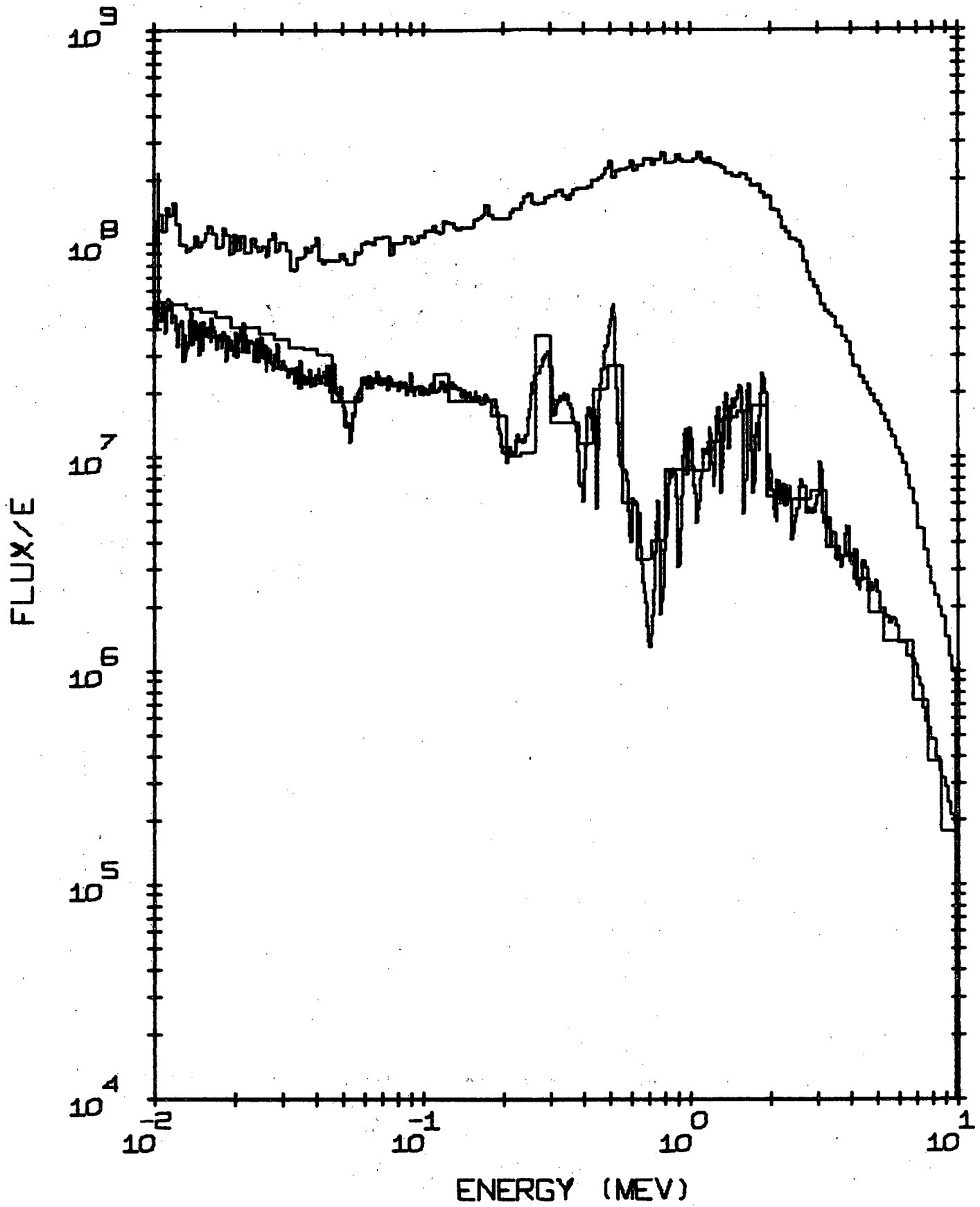## SOURCE, AND R=18·5 IN, MU=1·00

Figure 3

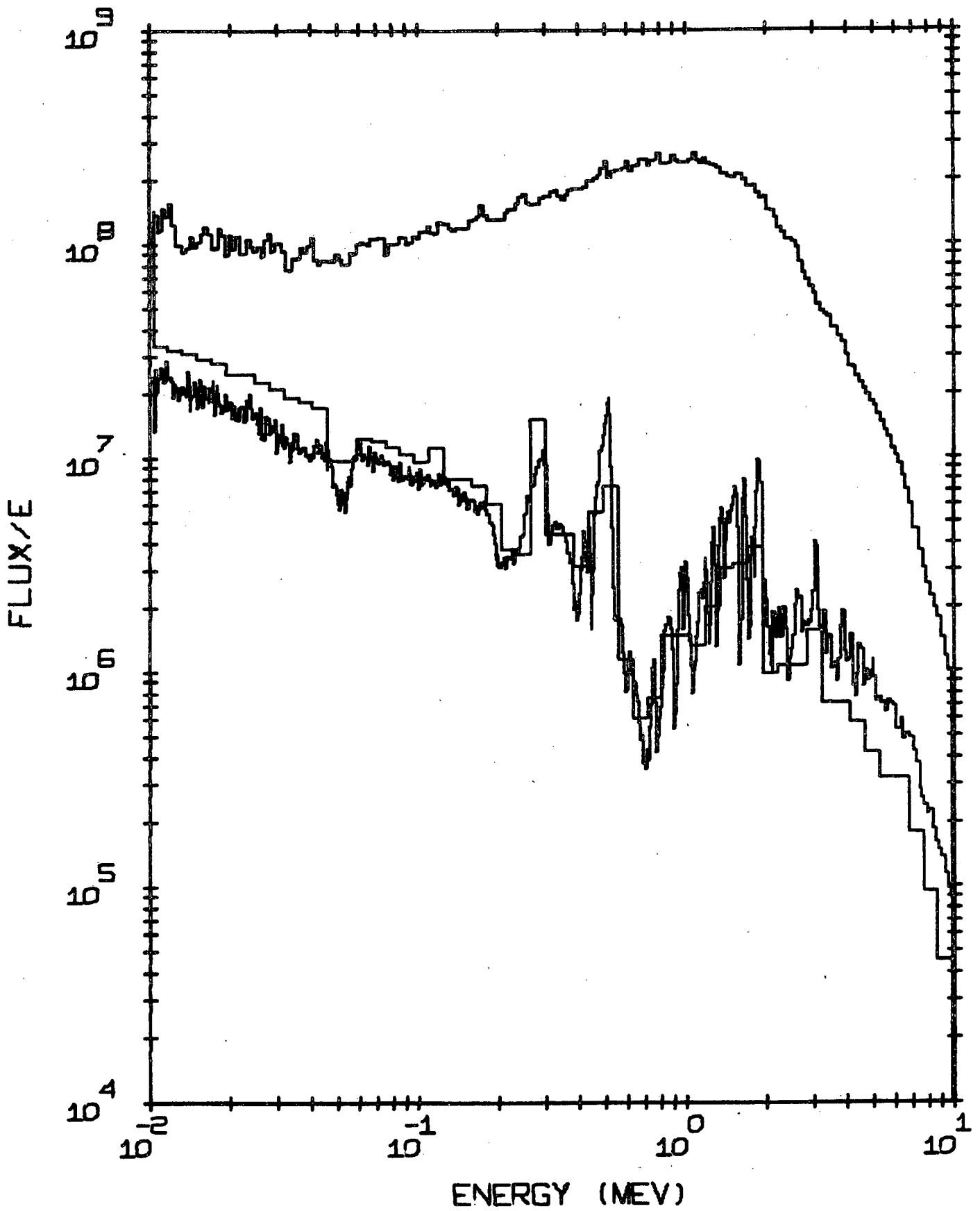SOURCE, AND R=26.5 IN, MU=1.00

Figure 4

REACTOR PHYSICS AND ENGINEERING - THEORETICAL

REACTOR THEORY AND ANALYSIS
M. Becker

Calculations have been performed for a depleted uranium assembly using data containing n;γ,n' cross sections supplied by J. Neill of Gulf Radiation Technology. An assessment of these data has been made and a paper prepared for publication in co-operation with Dr. N. N. Kaushal. Figure 1 shows a typical comparison with experiment. Note the very large predicted flux increment at low energy. Figure 2 shows, by contrast, a comparison using "ordinary" ENDF/B data. It is our judgment that these (n;γ,n') data should not be incorporated into data files.

Progress continues to be made in the continuous slowing down integral transport treatment of interfaces (with G. Epstein). A variety of modifications to the theory have led to continually improved results.

The re-entrant hole study in curved geometry has been completed. The study indicates that angular effects around the hole lead to significant re-entrant hole perturbations at high energies, particularly in backward directions. This conclusion is consistent with high energy discrepancies observed in iron and aluminum.

A preliminary study of the theoretical foundation of the tangent-θ method of subcriticality measurement has been completed. A draft report has been forwarded to AEC. In essence, the study identified the assumptions implicit in the method and indicated the types of corrections needed to convert measured quantities to kinetic parameters of interest. It was determined that for thermal reactor assemblies, the corrections were modest and easy to apply. However, for fast reactor applications, the assumptions were more substantial and a more intensive study would be required to demonstrate whether corrections could be made reliably. It was concluded that the incentive for the tangent-theta method was sufficient to warrant more intensive study for fast reactor applications.

FIGURE CAPTIONS

Fig. 1   Comparison of Theory and Experiment Without $(n;\gamma,n')$
Reaction.

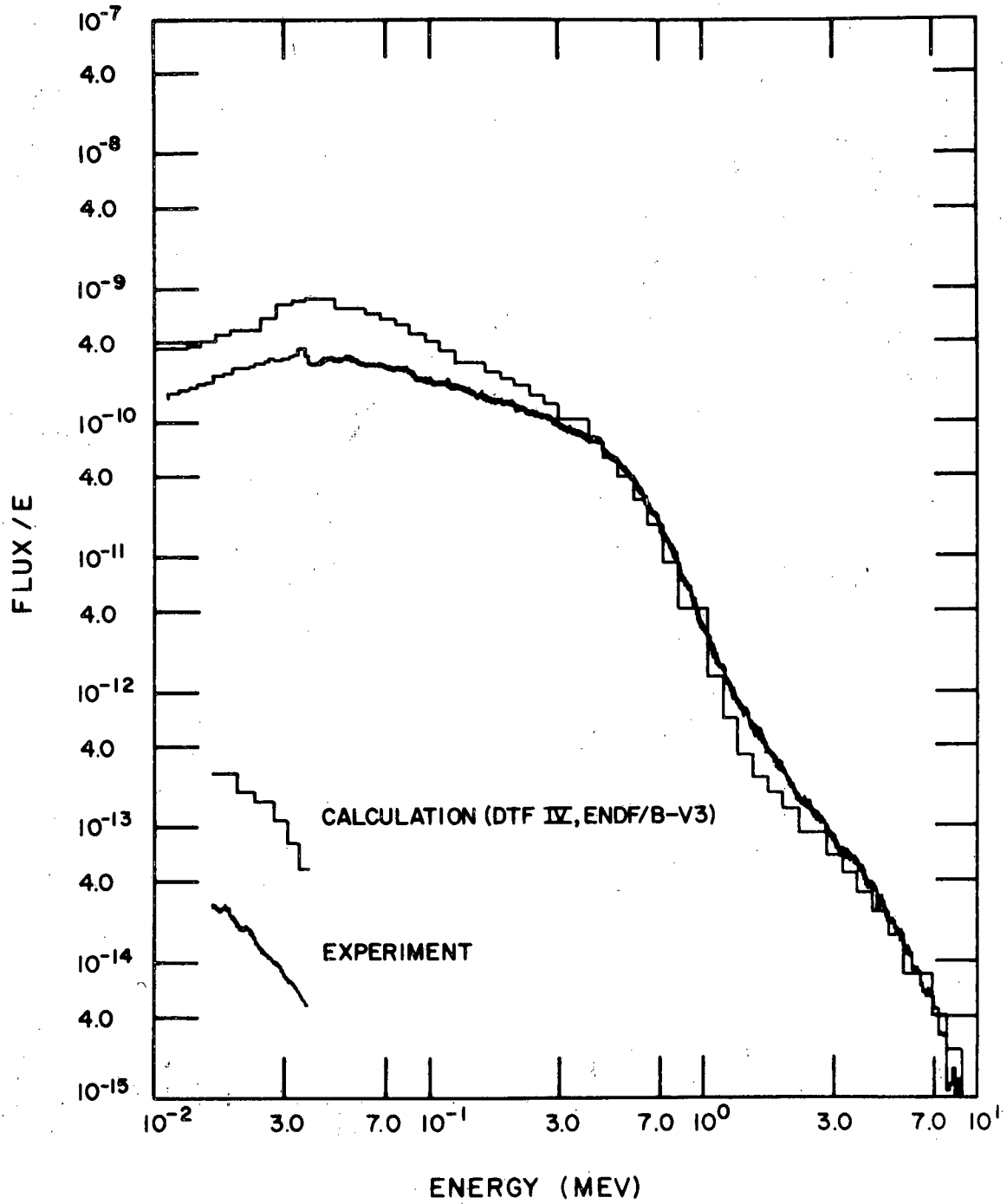Fig. 2   Comparison of Theory and Experiment With $(n;\gamma,n')$
Reaction.

NEUTRON SPECTRUM IN DEPLETED URANIUM (R=10 inch, $\mu = 0$)
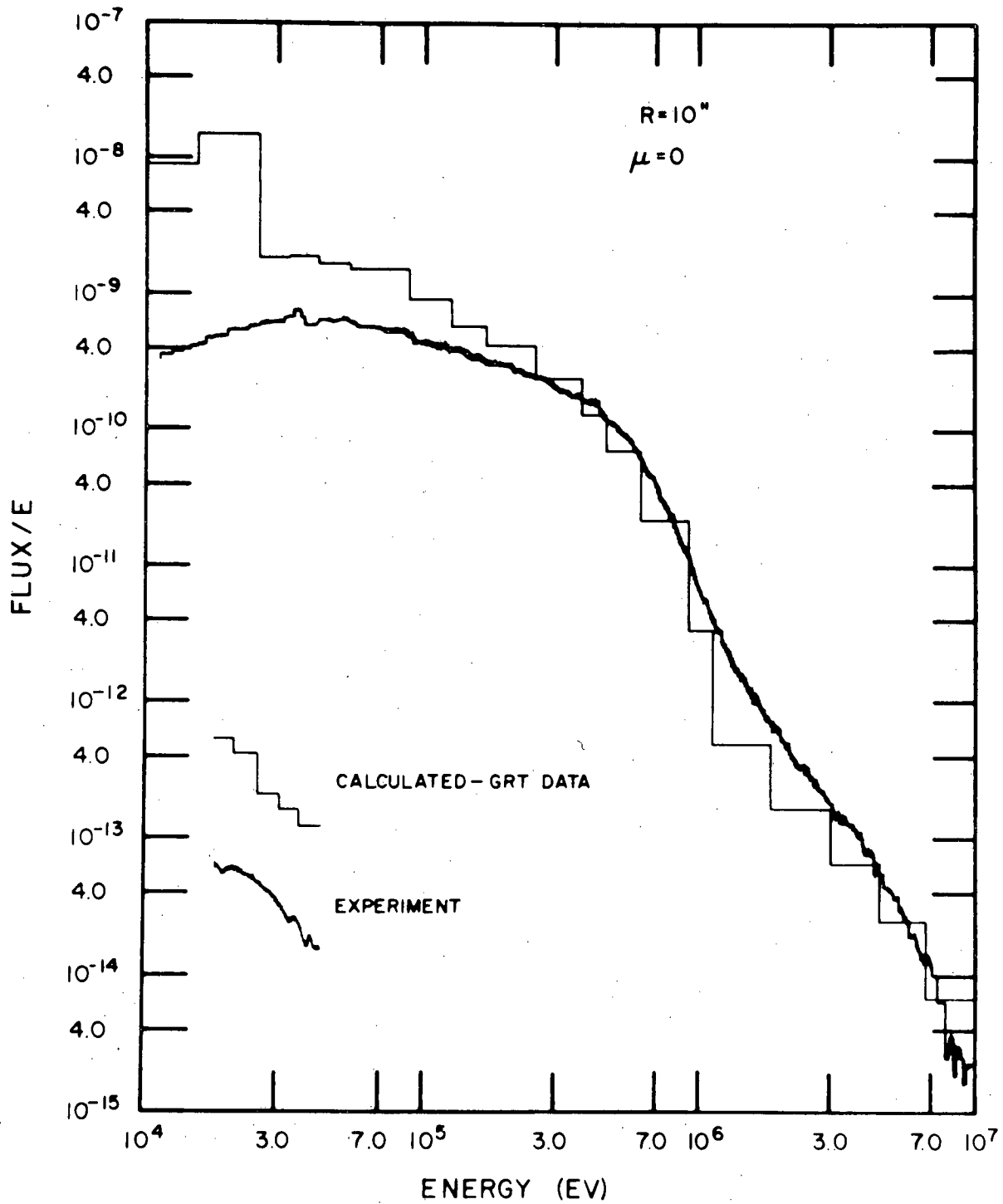

Figure 1

NEUTRON SPECTRUM IN DEPLETED URANIUM

Figure 2

INSTRUMENTATION DEVELOPMENT

INCREASED LINAC BEAM CURRENT WITH A MODEL 12 GUN

W. R. Moyer, J. R. Tatarczuk and R. C. Block

An RPI designed pulser and an ARCO Model 12 high current electron gun were recently installed in the LINAC to increase the peak electron beam current on target. The new pulser is capable of emitting 40 amperes into a 50 ohm resistive load, matching the characteristics of the Model 12 cathode under high current operation.

The pulser consists of (i) a pulse-forming network composed of a pair of Raytheon RT 3333 avalanche transistors in series plus selected lengths of open-ended coaxial cable, (ii) an intermediate pulse amplifier composed of a Machlett ML-8538 planar triode and (iii) a final pulse amplifier composed of four ML-8538 triodes in parallel. Rise and fall times of ~2 nsec were achieved over a range of pulse widths (FWHM) from ~5 to 200 nsec.

A maximum peak beam current of 6 amperes was measured on target (for ≤40 nsec pulse widths); whereas, the total peak emission from the gun was about 25 amperes. Recent tests at the Argonne linear accelerator[*] show that a higher powered buncher should increase the peak target current from 6 amperes to at least 20 amperes.

The pulser and Model 12 gun have been in service for over five months and have functioned very reliably. The gun (while cold) was let down to atmospheric pressure three times during this period, and each time the gun reactivated and returned to normal operation.

---

[*]G. Mavrogenes (private communication)